

Quasi-stationary States of Two-Dimensional Electron Plasma Trapped in Magnetic Field

Ryo KAWAHARA* and Hiizu NAKANISHI†

Department of Physics, Kyushu University 33, Fukuoka 812-8581

(Received December 2, 2018)

We have performed numerical simulations on a pure electron plasma system under a strong magnetic field, in order to examine quasi-stationary states that the system eventually evolves into. We use ring states as the initial states, changing the width, and find that the system evolves into a vortex crystal state from a thinner-ring state while a state with a single-peaked density distribution is obtained from a thicker-ring initial state. For those quasi-stationary states, density distribution and macroscopic observables are defined on the basis of a coarse-grained density field. We compare our results with experiments and some statistical theories, which include the Gibbs-Boltzmann statistics, Tsallis statistics, the fluid entropy theory, and the minimum enstrophy state. From some of those initial states, we obtain the quasi-stationary states which are close to the minimum enstrophy state, but we also find that the quasi-stationary states depend upon initial states, even if the initial states have the same energy and angular momentum, which means the ergodicity does not hold.

KEYWORDS: non-neutral plasma, two-dimensional turbulence, numerical simulation, long-range force, nonextensive system,

1. Introduction

A system with long-range interaction behaves quite differently from that with short-range interaction because the total energy is not proportional to the system size and the thermodynamic limit cannot be defined in an ordinary sense. In such a case, even a small subsystem of a large system may not obey the Boltzmann statistics because the subsystem interacts strongly with the rest of the system and its energy depends on the size of the whole system.

An example of such systems is pure electron plasma, where the electrons interact via Coulomb's law. By applying a strong magnetic field to the system, one can confine the electrons in a container for quite a long time, and examine quasi-stationary states of the system.

The system can be described by the two-dimensional (2-d) Euler equation with vorticity of the same sign if the finite Larmor radii of electrons are ignored; thus, its dynamics is analogous to that of 2-d incompressible inviscid fluid. In the 2-d fluid systems, the dynamics of vortices are known to be important in understanding the system behavior, as is seen in large-scale geophysical flows of high Reynolds number.

A system described by the 2-d Euler equation usually develops a fine vorticity structure by complex stretching and folding of the vorticity field, which results in finer and finer structures as the system evolves, but this does not usually lead to a fractal structure in stationary states; the fine structure eventually becomes too small to observe for any realistic observation with finite resolution; thus, quasi-stationary states observed in experiments and simulations usually have a rather smooth global structure, which may be predicted by some statistical methods.

Statistical theories of the 2-d perfect fluid originate from Onsager's work on the point vortex model.¹⁾ Since this model is described by a Hamiltonian, he has introduced the "temperature" in a microcanonical ensemble by taking the derivative of the logarithm of the number of states with respect to the total energy. In particular, in the case of "negative temperature", this theory predicts that small vortices merge together and eventually self-organize into a large single cluster.

In some simulations, the connection between the point vortex system and Onsager's theory has been investigated, and the result shows that, for the three-particle case, the initial state in the negative temperature region leads to the chaotic motion of particles.²⁾ A related result that the sign of the temperature affects the dynamics of the system has been also obtained for the system which contains particles with both signs of the vorticity.³⁾

Since Onsager, many theories have been proposed so far.⁴⁾ Some of them are based on maximization of the entropy,⁵⁻⁸⁾ while others are based on minimization of the enstrophy.⁹⁾ Most of the theories predict the formation of a large single cluster as the equilibrium state. However, experimental tests of the theories are difficult with an actual 2-d fluid, and the 2-d electron plasma system can be used to test such theories.

In 1994, an experiment was performed by Huang and Driscoll using 2-d electron plasma.¹⁰⁾ The results suggest that the quasi-stationary state of the 2-d electron plasma system is described by the minimum enstrophy theory and cannot be explained by any of the maximum entropy theories. This is particularly interesting because the minimum enstrophy state has been shown to be the maximum Tsallis entropy state with $q = 1/2$ in the Tsallis statistics, which has been developed to describe nonextensive systems.¹¹⁾

Numerical simulations on the 2-d electron plasma sys-

*E-mail : ryokawa@stat.phys.kyushu-u.ac.jp

†E-mail : naka4scp@mbox.nc.kyushu-u.ac.jp

tem have been performed. The minimum enstrophy state is also observed in simulation study using the same initial states as those in the experiment.¹²⁾ However, the initial-state dependence of such a stationary state has not been tested systematically. The validity of the minimum enstrophy theory has been tested by some authors, and it was claimed that the experimentally obtained density profile appears to be the minimum enstrophy state only because the mixing in the core and peripheral regions of the vortex cluster has not been completed yet.¹³⁾

Another kind of quasi-stationary state, called the vortex crystal state, has been found in experiments.^{14, 15)} The vortex crystal is analogous to the coherent vortex structure in 2-d turbulent flow,¹⁶⁾ but the vortex crystal state has not been described by any known statistical theories; it is described only phenomenologically.¹⁷⁾

In numerical simulations, the existence of the vortex crystal state has been confirmed and the relaxation process to it has been studied. It has been shown that the vortex crystal state is sensitive to the small difference in initial states, and is stabilized by background vortices.¹⁸⁾ The vortex crystal state is realized not only with a large number of particles but also with only several hundred particles. In the simulation, the interaction between vortex clumps and background vortices is also found to be important; there are exchanges of energy and particles between them even after the formation of the vortex crystal state.²⁾ The effects of background vortices in the vortex crystal state, such as the dynamics of clumps and the formation of a regular structure, have also been intensively studied in experiments.^{19–21)}

In this study, we investigate the quasi-stationary states of the two-dimensional pure electron plasma under a strong magnetic field by numerical simulation. With our numerical results, we examine several statistical theories for the stationary state.

The paper is organized as follows: In §2, we introduce the 2-d electron plasma system under a magnetic field and define a model. In §3, we briefly review some statistical theories. The simulation method and results are described in comparison with the statistical theories in §4, and the summary and discussion are given in §5.

2. Model System and its Behavior

The system we consider is a pure electron plasma system in a cylindrical container with a uniform external magnetic field along its axis; in a certain experimental situation,^{10, 14, 15)} the system behaves like a 2-d one in the plane perpendicular to the axis; we investigate this situation in the following.

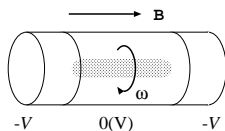


Fig. 1. Schematic diagram of Malmberg trap of pure electron plasma.

2.1 Equations of motion

We assume that the magnetic field is strong enough for the radii of cyclotron motion to be ignored; then the velocity \mathbf{v}_i of the i -th electron at \mathbf{r}_i within the plane is given by the drift velocity of the guiding center

$$\mathbf{v}_i = \frac{\mathbf{E}(\mathbf{r}_i) \times \mathbf{B}}{B^2} \quad (1)$$

under the existence of the electric field $\mathbf{E}(\mathbf{r})$ perpendicular to the uniform magnetic field \mathbf{B} . In the present situation, \mathbf{E} is generated by the electrons themselves, as

$$\mathbf{E} = -\text{grad}\phi, \quad \nabla^2\phi = \frac{e}{\epsilon_0} \sum_i \delta(\mathbf{r} - \mathbf{r}_i(t)), \quad (2)$$

where grad and ∇^2 are the 2-d gradient and Laplacian, ϕ is the 2-d electric potential with the boundary condition $\phi = 0$ at the container wall, e is the charge of an electron, and ϵ_0 is the dielectric constant of vacuum. Thus, the electrons do not repel each other and the plasma can be confined in a container (Malmberg trap, Fig. 1). The system described by eqs. (1) and (2) is called the point vortex system, because the interaction between the electrons is analogous to that between vortices.

If the system contains macroscopic numbers of electrons and can be described by a smooth density field $n(x, y)$, then the density field follows the following partial differential equations:

$$\frac{Dn}{Dt} \equiv \frac{\partial n}{\partial t} + \mathbf{v} \cdot \nabla n = 0, \quad (3)$$

$$\mathbf{v} = \hat{\mathbf{z}} \times \nabla\phi = \left(-\frac{\partial\phi}{\partial y}, \frac{\partial\phi}{\partial x} \right), \quad (4)$$

$$\nabla^2\phi = n, \quad (5)$$

where $\hat{\mathbf{z}}$ denotes the unit vector perpendicular to the plane and ∇ is the 2-d nabla. We have normalized the potential and density as $(1/B)\phi \mapsto \phi$ and $(e/\epsilon_0 B)n \mapsto n$.

It can be shown that the density field n is equal to the vorticity $\omega(\mathbf{r}) \equiv (\nabla \times \mathbf{v})_z$ of the 2-d velocity field \mathbf{v} and the velocity field \mathbf{v} is solenoidal ($\nabla \cdot \mathbf{v} = 0$); therefore, the set of equations (3)–(5) is the same with that of the Euler equation for the 2-d incompressible inviscid fluid with a free-slip (no-stress) boundary condition, but the vorticity takes only a positive value in the present system.

Note that the density field

$$n(\mathbf{r}) = \sum_i \delta(\mathbf{r} - \mathbf{r}_i(t)) \quad (6)$$

with $\mathbf{r}_i(t)$ being a solution of eqs. (1) and (2) gives a singular solution for eqs. (3)–(5).

Although the dynamics given by eqs. (1) and (2) is not Newtonian, it can be expressed in the form of canonical equations,

$$\frac{dx_i}{dt} = \frac{\partial H}{\partial y_i}, \quad \frac{dy_i}{dt} = -\frac{\partial H}{\partial x_i}, \quad (7)$$

with the Hamiltonian H ,

$$\begin{aligned} H &= -\frac{1}{2} \sum_i^N \sum_{j \neq i}^N G(\mathbf{r}_i, \mathbf{r}_j) - \frac{1}{2} \sum_i^N G_m(\mathbf{r}_i, \mathbf{r}_i) \\ &= -\frac{1}{2} \sum_i^N \phi_i(\mathbf{r}_i), \end{aligned} \quad (8)$$

where $G(\mathbf{r}_i, \mathbf{r}_j)$ is the 2-d Green function for the electric potential, $G_m(\mathbf{r}, \mathbf{r}')$ is the electric potential at \mathbf{r} brought about by the mirror charge induced by the charge at \mathbf{r}' to satisfy the boundary condition, and $\phi_i(\mathbf{r})$ is the electric potential due to all the electrons except for the i th one. The Green function satisfies

$$\nabla^2 G(\mathbf{r}, \mathbf{r}') = \delta(\mathbf{r} - \mathbf{r}'), \quad (9)$$

under an appropriate boundary condition. In the present case, we consider that the system is in a cylindrical container with the radius R_w ; then ϕ_i is given by²⁾

$$\begin{aligned} \phi_i(\mathbf{r}) &\equiv +\frac{1}{2\pi} \sum_{j \neq i}^N \ln |z - z_j| \\ &\quad - \frac{1}{2\pi} \sum_j^N \left[\ln \left| z - \frac{R_w^2}{z_j^*} \right| + \ln \frac{|z_j|}{R_w} \right], \end{aligned} \quad (10)$$

where $z = x + iy$ and z^* is the complex conjugate of z ; the second term corresponds to the potential brought about by the mirror charges.

2.2 Constants of dynamics

The Hamiltonian H is a constant of the dynamics, and is expressed in terms of the field variables as

$$\begin{aligned} H &= -\frac{1}{2} \int d^2\mathbf{r} \int d^2\mathbf{r}' n(\mathbf{r}) n(\mathbf{r}') G(\mathbf{r}, \mathbf{r}') \\ &= -\frac{1}{2} \int d^2\mathbf{r} n(\mathbf{r}) \phi(\mathbf{r}) \\ &= \int d^2\mathbf{r} \frac{1}{2} v^2(\mathbf{r}), \end{aligned} \quad (11)$$

which corresponds to the total energy.

In the case of a system with circular symmetry, the

total angular momentum L around the center of the system,

$$\begin{aligned} L &\equiv \sum_i^N r_i^2 \\ &= \int d^2\mathbf{r} r^2 n(\mathbf{r}) \\ &= \int d^2\mathbf{r} (\mathbf{r} \times \mathbf{v}(\mathbf{r}))_z, \end{aligned} \quad (12)$$

is also a constant of the dynamics.

In addition to the above two quantities, if the system is described by a smooth density field that satisfies eqs. (3)–(5), it can be shown that the integral Z of any function f of n ,

$$Z \equiv \int d^2\mathbf{r} f(n(\mathbf{r})), \quad (13)$$

is a constant of the dynamics; this is called a Casimir constant.^{11,22)}

Out of the Casimirs, the enstrophy Z_2 ,

$$Z_2 \equiv \frac{1}{2} \int d^2\mathbf{r} n^2(\mathbf{r}), \quad (14)$$

and the one-body entropy S_1 ,

$$S_1 = - \int d^2\mathbf{r} n(\mathbf{r}) \log n(\mathbf{r}), \quad (15)$$

are of particular interest.

Although any Casimir is a conserved quantity for the dynamics given by eq. (3), it is often not conserved in simulations and experiments¹⁰⁾ (Fig. 2); this is because the field quantities are defined only at a finite resolution by averaging over a mesh with a finite size.¹⁸⁾

When the density function can be measured in a fine-enough resolution compared with the density structure, the value of a Casimir should not depend on the size of the mesh, but it depends on the resolution when there exists a density structure smaller than the mesh size. The present system often develops very quickly a fine structure in density by stretching and folding. The smallest length scale of the structure appears to decrease exponentially in time, in which case the value of the coarse-grained Casimir is not conserved as long as the mesh size is finite.

Note that the density field in the quasi-stationary state, if coarse grained over these evolving small length scales, usually has a smooth structure in the scales comparable to the system size; thus, the value of enstrophy or any Casimir should be well defined for the coarse-grained field. This is because the stretching and folding do not lead to a fractal structure in simulations and experiments; all the structures except some large structures comparable to the system size are transferred to finer and finer scales as they evolve; thus, we find that the scales of these large structures are well separated from the fine scale in the quasi-stationary state. Since the fine structure eventually becomes invisible for any measurement with a finite resolution, the coarse-grained density field has a fairly simple structure with the size comparable to the system size, which is independent of the resolution

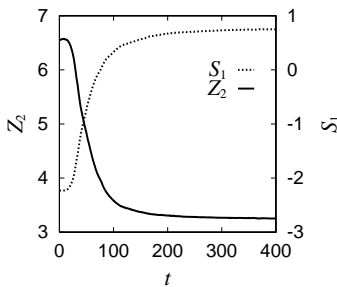


Fig. 2. Time evolution of two Casimirs in simulation: the dotted line and dashed line represent the enstrophy Z_2 and entropy S_1 , respectively. The initial distribution is ring shaped with $R_1/R_0 = 0.6$. See Fig. 6 for the meaning of the parameter. These observables are calculated on the basis of a coarse-grained density field using a finite-sized mesh with a resolution of 256×256 .

of measurement as long as the mesh size is finite and sufficiently smaller than the system size.

This is shown in Fig. 3, where the time developments of enstrophy are plotted using three different mesh sizes for a single simulation. The initial and transient values are quite different from each other, but the values for the quasi-stationary state become closer. Note that the rate of enstrophy change in the transient is almost independent of the mesh size of density coarse graining.

2.3 Stability and evolution of states

It can be shown that the rotationally symmetric state with a decreasing density n as a function of r is not linearly unstable and is numerically stable. On the other hand, the ring state, where the electrons are distributed in a ring-shaped region, is linearly unstable, and the instability is called diocotron instability.²³⁾

Figure 4 shows two examples of time sequences which start from unstable initial states and lead to two types of quasi-stationary states; the sequence in Fig. 4(a) starts from a single-ring configuration, which destabilizes owing to mode three, and eventually falls into a singly peaked stable density distribution. In the case of Fig. 4(b), a double-ring initial configuration results in instability owing to a higher mode to break into many vortices, which merge occasionally while they undergo a collective chaotic motion, and eventually several surviving vortices form a regular structure, which does not undergo further change during our simulation time; this state is called a vortex crystal state.¹⁴⁾

These quasi-stationary states are in general not the equilibrium states. In our preliminary simulations, it is observed that if there are only a small number of particles (for example, several hundreds), the system evolves very slowly in time after the quasi-stationary states are attained. However, for a large number of particles as in experiments and current simulations, time evolution after entering the quasi-stationary state is hardly observed.

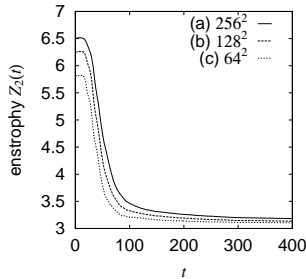


Fig. 3. Time evolution of enstrophy Z_2 of single simulation run with several resolutions of coarse-grained mesh: The macroscopic initial distribution is the same as in Fig. 2. The resolution of the VIC cell necessary to solve Poisson's equation is 512×512 (see §4.1 for the meanings of parameters). The resolution of density observation is 256×256 , 128×128 and 64×64 for (a)–(c), respectively.

3. Statistical Theories for Quasi-Stationary States

As explained in §2.2, we usually observe the system through the coarse-grained mesh because we are interested in the macroscopic structures of the system.

After the complex stretching and folding of the density structure, only a fine structure and a smooth structure are left in the “true” density distribution at the late stage of the evolution. Thus, the coarse-grained density field reaches the quasi-stationary states, which only has the smooth structure of a simple density field.

Although the dynamics of the present system is highly nonlinear and unpredictable, quasi-stationary states may be predicted by a simple principle; actually, there have been several statistical theories developed to predict the vortex cluster as a quasi-stationary state using variational methods.⁴⁾ We briefly review some of them in this section.

3.1 Maximum one-body entropy state

Although the one-body entropy S_1 (eq. (15)) is a Casimir constant, in actual simulations, the coarse-grained one-body entropy shows a rapid initial increase and reaches a steady value (Fig. 2); thus, the coarse-grained density distribution n of the steady state might be given by maximizing S_1 , keeping the total number of electrons N , the total energy H , and the total angular momentum L constant. Using the variational method,

$$\delta(S_1 - aN - bH - cL) = 0, \quad (16)$$

where a , b and c are Lagrange multipliers and determined from the constraints.¹⁰⁾ If the energy H of eq. (11) is evaluated ignoring electron correlation, then we obtain

$$n(\mathbf{r}) = \exp(-1 - a + b\phi(\mathbf{r}) - cr^2). \quad (17)$$

From eq. (5), ϕ satisfies

$$\nabla^2 \phi(\mathbf{r}) = \exp(-1 - a + b\phi(\mathbf{r}) - cr^2), \quad (18)$$

which can be solved numerically.

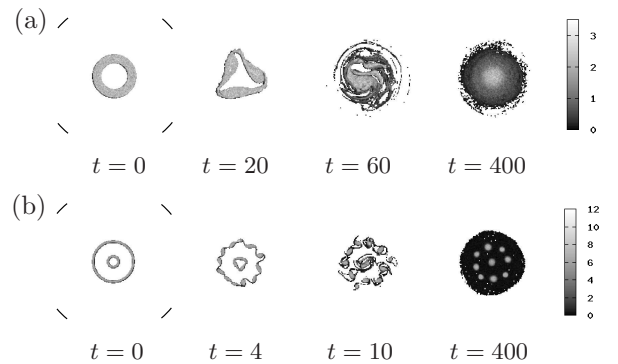


Fig. 4. Time evolutions of electron density distribution from single-ring initial state (a), and double-ring initial state (b). Initial distributions are shown in the left-most figures and quasi-stationary states are shown in the right-most figures. The conductor wall boundary is expressed by the black curve in the left-most figure.

3.2 Maximum fluid entropy state

The fluid entropy^{7,8,24)} is the entropy defined in terms of the probability distribution $p(\sigma_j; \mathbf{r}_i)$ of the discretized vorticity σ_j in the coarse-grained cell at \mathbf{r}_i as

$$S_{\text{fluid}} \equiv - \sum_{\mathbf{r}_i} \sum_{\sigma_j} p(\sigma_j; \mathbf{r}_i) \ln p(\sigma_j; \mathbf{r}_i), \quad (19)$$

where σ_j 's are the strengths of microscopic vortex elements. This fluid entropy has been introduced on the basis of the idea of counting the number of configurations of vortices over discretized space.²⁴⁾

The probability distribution $p(\sigma_j; \mathbf{r}_i)$ satisfies the normalization

$$\sum_{\sigma_j} p(\sigma_j; \mathbf{r}_i) = 1 \quad (20)$$

at each \mathbf{r}_i , and is related to the total numbers of vortices $g(\sigma_j)$ of the strength σ_j by

$$g(\sigma_j) = \sum_{\mathbf{r}_i} p(\sigma_j; \mathbf{r}_i); \quad (21)$$

it is assumed that $g(\sigma_j)$ does not change because the strength of each vortex does not change.

The coarse-grained density (vorticity) $n(\mathbf{r}_i)$ at the cell \mathbf{r}_i is given by

$$n(\mathbf{r}_i) = \sum_{\sigma_j} p(\sigma_j; \mathbf{r}_i) \sigma_j. \quad (22)$$

The maximum fluid entropy state is given by maximizing eq. (19) over a variation of $p(\sigma_j; \mathbf{r}_i)$ under the constraints of eqs. (20) and (21) in addition to H and L . This gives

$$p(\sigma_j; \mathbf{r}_i) = \frac{\exp[-\gamma(\sigma_j) + b\phi(\mathbf{r}_i) - c\sigma_j^2]}{\sum_{\sigma_k} \exp[-\gamma(\sigma_k) + b\phi(\mathbf{r}_i) - c\sigma_k^2]}, \quad (23)$$

where $\gamma(\sigma_j)$, b and c are Lagrange multipliers. Note that the total number of particles N is given by

$$N = \sum_{\sigma_i \neq 0} g(\sigma_i); \quad (24)$$

therefore, we need not include N as a constraint. In the continuum limit in space, combining this with eqs. (22) and (5), the potential ϕ can be solved numerically.

In principle, these constants and the values of σ_j 's should be determined by the initial states of 2-d fluid. However, there is ambiguity in the values of σ_j 's since we only know the coarse-grained information of the initial states, $n(\mathbf{r})$, while different sets of σ_j 's can give the same $n(\mathbf{r})$. To apply the theory to our simulation of 2-d electron plasma, we take the values of σ_j 's to be those of the coarse-grained density of the initial states, as Huang and Driscoll did in their analysis of the experiment.¹⁰⁾

3.3 Minimum enstrophy state

Another Casimir constant, the enstrophy Z_2 defined by eq. (14), is known to cascade towards smaller length scales,^{25,26)} and be dissipated in the regime where eq. (3) is not exact; numerically, the coarse-grained enstrophy has been shown to decrease initially until it reaches a steady value; thus, coarse-grained density field n for the steady states could be given by minimizing Z_2 within

given values of N , H and L as in the maximum entropy state.^{9,10)} This gives

$$n(\mathbf{r}) = a - b\phi(\mathbf{r}) + cr^2, \quad (25)$$

where a , b , and c are again the Lagrange multipliers and determined by the constraints. Operating the 2-d Laplacian on both-hand sides of eq. (25) and assuming $n(\mathbf{r})$ is axisymmetric, we obtain

$$\frac{d^2 n}{dr^2} + \frac{1}{r} \frac{dn}{dr} + bn - 4c = 0. \quad (26)$$

This is the 0th-order Bessel equation; therefore, the solution is given by the Bessel function. The problem, however, is that the Bessel function takes values with the both signs but the density $n(\mathbf{r})$ should be always positive or zero. This means that the function that minimizes Z_2 is outside the domain of physically allowed functional space. In such a case, the function that minimizes Z_2 within the physical domain is the one at the edge of the physical domain in the functional space, i.e., the function that satisfies eq. (26) for the section of r where the solution is positive but is zero where it is negative.

For $b > 0$, which corresponds with the higher energy case, we employ the solution

$$n(r) = \begin{cases} \alpha[J_0(\beta r) - J_0(\beta r_0)], & (r < r_0) \\ 0, & (r_0 < r) \end{cases} \quad (27)$$

where $J_0(x)$ is the 0th-order Bessel function, and α , β , and r_0 are determined by the constraints. The parameter r_0 is a cutoff length, which is introduced to avoid a negative density region,^{9,10)} where it is assumed that the region of $n = 0$ is only in the outer part of the system, $r_0 < r$. This type of solution is called the restricted minimum enstrophy model.¹⁰⁾

For $b < 0$ (the lower energy case), the solution is

$$n(r) = \begin{cases} \alpha[I_0(\beta r) - I_0(\beta r_0)], & (r < r_0) \\ 0, & (r_0 < r) \end{cases} \quad (28)$$

where $I_0(x) = J_0(ix)$ is the 0th-order modified Bessel function. This solution gives the pancake shape of $n(\mathbf{r})$ in the limit of $\beta \rightarrow \infty$ ($\alpha < 0$), which corresponds to the minimum energy state.

Actually, it has been shown experimentally that there are some cases in which quasi-stationary states are very close to the minimum enstrophy states.¹⁰⁾

It has been pointed out that the minimum enstrophy state is the state that maximizes Tsallis entropy

$$S_q = \frac{1}{1-q} \int d^2 \mathbf{r} [p^q(\mathbf{r}) - p(\mathbf{r})] \quad (29)$$

with $q = 1/2$ in the Tsallis statistics formalism.¹¹⁾

4. Simulations

4.1 Method

We simulate eqs. (1) and (2) using a variation of the point vortex method;²⁷⁾ for a given set of electron (or vortex) positions, we calculate the electron density $n(\mathbf{r})$ on a grid point by averaging over the cell; then Poisson's equation is solved to obtain the electrostatic potential $\phi(\mathbf{r})$, from which the electric field $\mathbf{E}(\mathbf{r})$ is calculated, and the electron positions are updated by eq. (1);

this is called the vortex-in-cell (VIC) simulation.^{18,28)} Numerical integration in time is performed using the second-order Adams-Bashforth-Adams-Moulton method and Poisson's equation is solved by an implicit method adopting multiple grids to accelerate the convergence.²⁹⁾

The effects of these simulation parameters, such as the resolution of the VIC cell necessary to solve Poisson's equation and the number of particles, are shown in Fig. 5. We see almost no difference among these three simulations of different VIC cell resolutions and numbers of particles. Thus, for singly peaked quasi-stationary states, simulation results are almost independent of these parameters.

For initial states which lead to vortex crystal states, however, the systems are sensitive to the microscopic difference of the initial states and may lead to macroscopically different density distributions of vortex crystal states because of the chaotic motion in the transient stage. In this case, the simulation results also depend on those simulation parameters, such as the VIC cell resolution, the number of particles and the random number sequence of the initial distribution. We do not focus on the sensitivity in the density distribution of vortex crystals since our aim on this study is to compare singly peaked quasi-stationary states of simulations with the statistical theories.

The following simulations are performed on the 256×256 grid with $N = 80 \times 10^3$ particles.

4.2 Results

4.2.1 General trends and classification of quasi-stationary states

We have systematically examined quasi-stationary states in the case where the system starts from the ring states with various ring widths (Fig. 6(a)); the initial ring state is the state where the electrons are distributed uniformly in the region $r \in [R_1, R_0]$, and the ratio R_1/R_0 is changed from 0 to 1. The total number of electrons N and the angular momentum L are fixed to $N = 80 \times 10^3$ and $L = \pi/2$ in all cases, but the energy H is an increasing function of R_1/R_0 ; namely, the energy is larger for

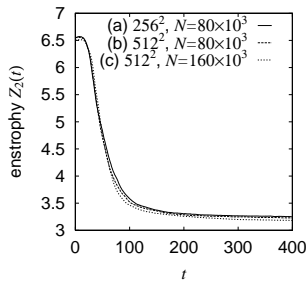


Fig. 5. Time evolution of enstrophy Z_2 for different VIC cell resolutions and numbers of particles: The macroscopic initial distribution is the same as in Fig. 2. For these three simulations, the density field is observed in the 256×256 mesh. The resolution of the VIC cell necessary to solve Poisson's equation and the number of particles are (a) 256×256 and $N = 80 \times 10^3$, (b) 512×512 and $N = 80 \times 10^3$, and (c) 512×512 and $N = 160 \times 10^3$, respectively

the thinner ring.

The results are summarized in Fig. 6(b).

In the case of the thinner-ring initial state with $0.8 \lesssim R_1/R_0 \leq 1$, after the diocotron instability, the system goes through the chaotic motion of electron clumps; the clumps merge occasionally and finally result in the vortex crystal state, which does not change any more. The number of clumps in the quasi-stationary state is very sensitive to the initial configuration because the clumps merge accidentally during chaotic motion; their final number depends even upon the microscopic positions of electrons in the initial states.

For smaller values of $R_1/R_0 \lesssim 0.8$, the quasi-stationary states are singly peaked stationary states with circular symmetry; in this regime, the quasi-stationary state is rather insensitive to the details of the initial state and does not depend upon the microscopic configuration. As the ratio R_1/R_0 decreases, the density distribution of the quasi-stationary state becomes flatter around the peak at the center, as can be seen in Fig. 7, the initial “pancake state” with $R_1/R_0 = 0$ is stable, and the system does not evolve at all.

For $R_1/R_0 \lesssim 0.5$, the minimum enstrophy state seems to give a reasonably good description of the quasi-stationary state (Fig. 7(b)), and for $R_1/R_0 \lesssim 0.3$, the minimum enstrophy state and maximum entropy state are not so different and both of them are close to the quasi-stationary state obtained from the simulations. (Fig. 7(a))

Note that the minimum enstrophy state has no physical solution with the present angular momentum for $R_1/R_0 \gtrsim 0.5$.¹⁰⁾

Actually, for $R_1/R_0 \approx 0$, all the statistical theories give the states that resemble each other very much and cannot be distinguished clearly; this is the result of the

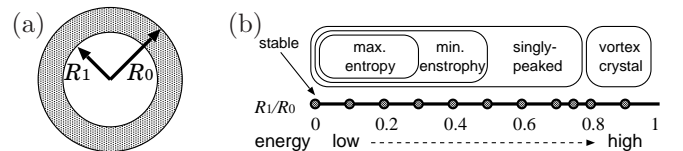


Fig. 6. (a) Initial ring state. (b) Schematic diagram of quasi-stationary states for various ring widths R_1/R_0 .

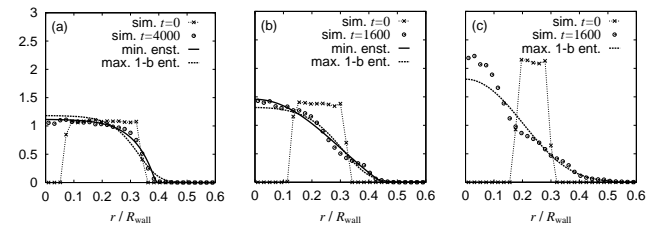


Fig. 7. Radial density distributions for stationary states from initial ring states with $R_1/R_0 = 0.2$ (a), 0.4 (b) and 0.6 (c). The value of the angular momentum is $L = \pi/2$ for all three cases, and the energies are $E = 2.062$ (a), 2.078 (b) and 2.113 (c). The minimum enstrophy state and maximum one-body entropy state are also shown except for $R_1/R_0 = 0.6$ (c), where no physical solutions of the minimum enstrophy state exist.

fact that, for $R_1/R_0 = 0$, the only possible state for the given energy and angular momentum is the initial pancake state; thus, all the statistical theories should give the same state with this initial state.

The minimum entropy state seems to give a better approximate state for $0.3 \lesssim R_1/R_0 \lesssim 0.5$ than the maximum entropy state. This is because the simulations give the quasi-stationary state with a steeper peak for a larger R_1/R_0 and the minimum entropy state tends to give the state with a steeper peak in n than the maximum entropy state (Fig. 7(b) and 7(c)).

On the other hand, it should be noted that there is a discrepancy between the minimum entropy states and the stationary states obtained by the simulations, if one compares them carefully; in the minimum entropy state, the tail of the density profile is cut off with a finite slope at a certain point, beyond which the density is zero, while in the simulations, the density goes to zero smoothly with the zero slope.

4.2.2 Ergodicity

Although the minimum entropy state generally gives a reasonable description for $R_1/R_0 \lesssim 0.5$ in the case of the ring initial state, the quasi-stationary states are not uniquely determined by the energy and angular momentum. The system can travel over only a subsection of the phase space at given values of energy and momentum; that is, the system is not ergodic.

This can be seen in Fig. 8, which shows the quasi-stationary states and the states given by the statistical theories for the two initial states with the same values of N , L and H , namely, the single-ring initial state with a finite density inside the ring (Fig. 8(a)), and the double-ring initial state (Fig. 8(b)).

When we try to fit these states to the ones from the statistical theories, we should note that the maximum one-body entropy states and minimum entropy states are the same for the two cases because they only depend on the values of N , L and H . The quasi-stationary states obtained by the simulations are clearly different, and the

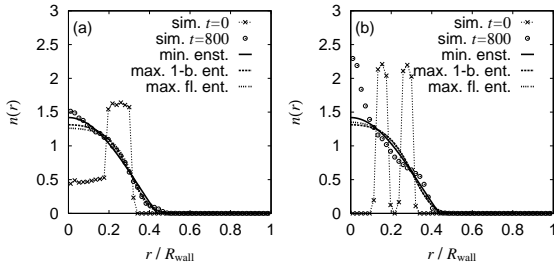


Fig. 8. Two different quasi-stationary states from two different initial states with the same energy $H = 2.078$ and angular momentum $L = \pi/2$: The initial states are the single ring with a finite interior density (a) and the double ring (b). The minimum entropy state, maximum one-body entropy state and maximum fluid entropy state are also shown; they are the same for both cases except for the maximum fluid entropy states; the maximum fluid entropy depends on the set of values σ_j , which is different for the two cases: $\sigma_0 = 0$, $\sigma_1 = 0.49$ and $\sigma_2 = 1.62$ for (a), and $\sigma_0 = 0$ and $\sigma_1 = 2.25$ for (b).

one from the single-ring-like state almost coincides with the minimum entropy state, while the quasi-stationary state from the double ring is different from both of the maximum entropy and minimum entropy states mainly because of the steep peak at the center.

To determine if there are any statistical theories that fit the quasi-stationary states from the double ring, we try the maximum fluid entropy state and maximum Tsallis entropy state, because these theories contain extra parameters other than the energy and angular momentum; therefore, they may be able to distinguish the two initial states.

The maximum fluid entropy state depends on the choice of a set of σ_j . In Fig. 8, we use the values determined from the initial density as shown in the figure caption. The resulting state, however, does not agree well with either of the stationary states as can be seen in Fig. 8.

Figure 9 shows the density profiles for the maximum Tsallis entropy states. A maximum Tsallis entropy state has a parameter q ; the state with $q = 1/2$ is the minimum entropy state and that with $q = 1$ is the maximum one-body entropy state. It can be seen that the state with a smaller value of q , such as $q = 1/3$ state, shows a fatter profile and is not closer to the simulation data in Fig. 8(b) than the $q = 1/2$ state, or the minimum entropy state. Actually, one can see that the state with $q \approx 0.53$ shows the steepest density profile, which turns out to be very close to the minimum entropy state. It has been shown³⁰⁾ that the peak density decreases monotonically as q increases in the parameter region $0.5 < q < 1.0$. Again, it is clear that we cannot fit the state to a maximum Tsallis entropy state with any choice of the parameter q .

4.2.3 Peak density in quasi-stationary state

There exists a high-density region around the center in the stationary state from the double ring in Fig. 8(b). This peaky profile cannot be fitted by any of the statistical theories we tried. The value of the peak density in the quasi-stationary state is approximately the same as that in the initial state. This property can be seen in other cases of Figs. 7 and 8 and in almost all the simulations we have carried out.

From the time developments of the states, it is conceivable that, during the relaxation process, the initial

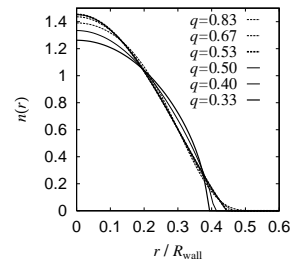


Fig. 9. Maximum Tsallis entropy states for various values of q with the same energy $H = 2.078$ and angular momentum $L = \pi/2$, which correspond to parameters of Fig. 8.

density is kept in the region of the peak density. The peak density in quasi-stationary states is never larger than that of initial states.

A similar feature has been observed in the vortex merger process in two-dimensional free decaying turbulence, where the vortices of both charges exist.^{16,31)}

5. Summary and Discussion

We have performed the numerical simulations on the two-dimensional point vortex model with a unit circulation of the same sign, in order to study the quasi-stationary states of pure electron plasma under a strong magnetic field, and have compared the coarse-grained density distribution of the quasi-stationary state with those of several statistical theories. By changing the radii ratio R_1/R_0 of the initial ring state, we found (i) for $0.8 \lesssim R_1/R_0 \leq 1$, the quasi-stationary state is a vortex crystal state and (ii) for $0 \lesssim R_1/R_0 \leq 0.8$, the quasi-stationary state is a singly peaked state. Further study in the parameter region of the singly peaked state revealed that (iii) for $0 \lesssim R_1/R_0 \leq 0.5$, the quasi-stationary singly peaked state is close to the minimum enstrophy state and (iv) for $0 \lesssim R_1/R_0 \leq 0.3$, the maximum entropy state and minimum enstrophy state are close to each other, and the quasi-stationary state is close to both of them.

These are consistent with the experiment,¹⁰⁾ where the quasi-stationary state has been found to be very close to the minimum enstrophy state when the initial state is prepared as the ring state.

Although these findings may provide evidence that the minimum enstrophy state is a good candidate for the statistical theory that can describe the quasi-stationary state for some parameter region, we have also found that this system lacks ergodicity; namely, the system does not necessarily fall into the same state even though its initial states have the same energy and angular momentum; thus, the statistical theory gives the same quasi-stationary state.

In some experiments¹⁴⁾ and simulations,^{12,18)} it has already been found that the vortex crystal state is sensitive to the microscopic difference in initial states and may lead to completely different quasi-stationary states. In the case where the quasi-stationary state is singly peaked, the quasi-stationary state does not depend on the microscopic details, namely, the position of each electron in the initial state, as long as the configuration gives the same coarse-grained density profile, but we still found that the quasi-stationary state depends on macroscopic differences in the initial state, such as the single- or double-ring state.

The nonergodicity of the system in the quasi-stationary state is not an artifact due to the finite-sized mesh used in the VIC method. As has been seen in §4.1, the obtained quasi-stationary state barely depends on the mesh size as long as it is fine enough.

On the other hand, our preliminary results suggest that these quasi-stationary states are not really stationary but undergo a very slow transient relaxation; the relaxation time seems to be proportional to the total number of particles when the time is measured in terms

of global rotation period. This indicates that the relaxation time required to access the “true” stationary state for systems of a large number of particles such as those in our simulations and experiments is much longer than the observation time, even longer than the time of electron confinement in experiments, which suggests that the true stationary state is hardly obtained in such systems and the quasi-stationary state is realized for quite a long time.

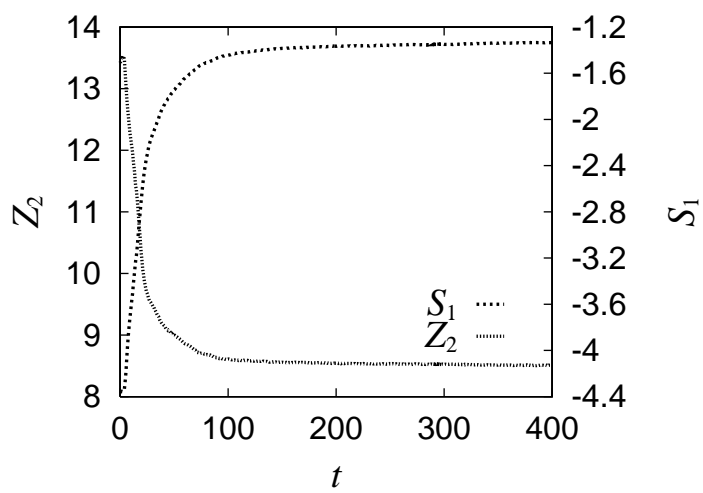
As we have mentioned in §4.2.3, there is a tendency that the peak density of the initial state is conserved. This property, the conservation of the highest density, may be one of the reasons that the quasi-stationary state is apparently very close to the minimum enstrophy state for a certain parameter region, because the minimum enstrophy state is realized only in the parameter region where the highest density in the minimum enstrophy state is nearly equal to the highest density in the initial state. To clarify this point, further study is required.

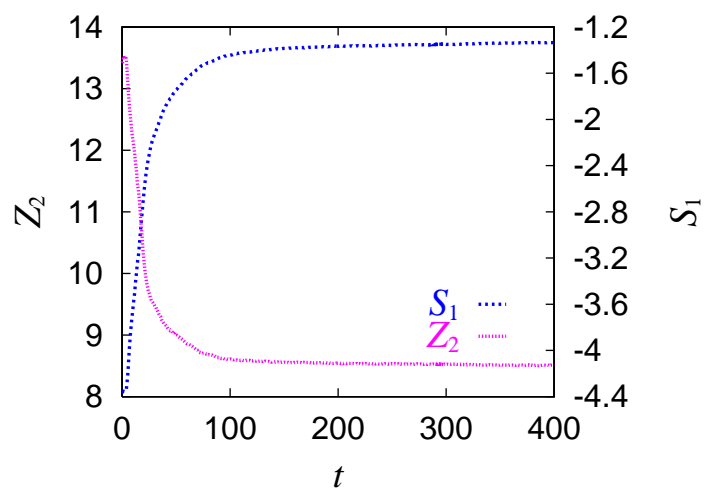
Acknowledgments

We would like to thank to Professor Y. Kiwamoto, Professor M. Sakagami, Dr. Y. Yatsuyanagi and T. Yoshida for valuable discussions and comments.

- 1) L. Onsager: *Nuovo Cimento (Suppl.)* **6** (1949) 279.
- 2) T. Yoshida and M. Sano: *J. Phys. Soc. Jpn.* **74** (2004) 587.
- 3) Y. Yatsuyanagi, Y. Kiwamoto, H. Tomita, M. M. Sano, T. Yoshida and T. Ebisuzaki: *Phys. Rev. Lett.* **94** (2005) 054502.
- 4) P. Tabeling: *Phys. Rep.* **362** (2002) 1.
- 5) G. Joyce and D. Montgomery: *J. Plasma Phys.* **10** (1973) 107.
- 6) S. Kida: *J. Phys. Soc. Jpn.* **39** (1975) 1395.
- 7) J. Miller, P. B. Weichman and M. C. Cross: *Phys. Rev. A* **45** (1992) 2328.
- 8) R. Robert and J. Sommeria: *Phys. Rev. Lett.* **69** (1992) 2776.
- 9) C. E. Leith: *Phys. Fluids* **27** (1984) 1388.
- 10) X.-P. Huang and C. F. Driscoll: *Phys. Rev. Lett.* **72** (1994) 2187.
- 11) B. M. Boghosian: *Phys. Rev. E* **53** (1996) 4754.
- 12) V. Pavlov, D. Buisine and S. Decossin: *Phys. Fluids* **14** (2002) 3937.
- 13) H. Brands, P. H. Chavanis, R. Pasmanter and J. Sommeria: *Phys. Fluids* **11** (1999) 3465.
- 14) K. S. Fine, A. C. Cass, W. G. Flynn and C. F. Driscoll: *Phys. Rev. Lett.* **75** (1995) 3277.
- 15) C. F. Driscoll, D. Z. Jin, D. A. Schecter, E. J. Moreau and D. H. E. Dubin: *Physica Scripta* **T84** (2000) 76.
- 16) G. F. Carnevale, J. C. McWilliams, Y. Pomeau, J. B. Weiss and W. R. Young: *Phys. Rev. Lett.* **66** (1991) 2735.
- 17) D. Z. Jin and D. H. E. Dubin: *Phys. Rev. Lett.* **80** (1998) 4434.
- 18) D. A. Schecter, D. H. E. Dubin, K. S. Fine and C. F. Driscoll: *Phys. Fluids* **11** (1999) 905.
- 19) A. Sanpei, Y. Kiwamoto, K. Ito and Y. Soga: *Phys. Rev. E* **68** (2003) 016404.
- 20) Y. Kiwamoto, K. Ito, A. Sanpei and M. Mohri: *Phys. Rev. Lett.* **85** (2000) 3173.
- 21) Y. Soga, Y. Kiwamoto, A. Sanpei and J. Aoki: *Phys. Plasmas* **10** (2003) 3922.
- 22) D. D. Holm, J. E. Marsden, T. Ratiu and A. Weinstein: *Phys. Rep.* **123** (1985) 1.
- 23) R. C. Davidson: *Theory of Nonneutral Plasmas* (W. A. Benjamin, Inc., Reading, Mass., Tokyo, 1987).
- 24) J. Miller: *Phys. Rev. Lett.* **65** (1990) 2137.
- 25) R. H. Kraichnan: *Phys. Fluids* **10** (1967) 1417.
- 26) G. K. Batchelor: *Phys. Fluids* **12** (1969) II-233.
- 27) A. Leonard: *J. Comput. Phys.* **37** (1980) 289.

- 28) C. K. Birdsall and A. B. Langdon: *Plasma Physics Via Computer Simulation* (Adam Hilger, Bristol, Philadelphia, New York, 1991).
- 29) W. H. Press, S. A. Tenkolsky, W. T. Vetterling and B. P. Flannery: *Numerical Recipe in FORTRAN (Second Edition)* (Cambridge University Press, Cambridge, New York, Melbourne, 1992).
- 30) C. Anteneodo and C. Tsallis: J. Mol. Liquids **71** (1997) 255.
- 31) M. V. Melander, N. J. Zabusky and J. C. McWilliams: Phys. Fluids **30** (1987) 2610.





energy 0 low -----> high 1

